

# Feasibility of estimation of vertical transverse isotropy from microseismic data recorded by surface monitoring arrays

Davide Gei<sup>\*</sup>, Leo Eisner<sup>†</sup> and Peter Suhadolc<sup>‡</sup>

*\*Istituto Nazionale di Oceanografia e di Geofisica Sperimentale (OGS)*

*Borgo Grotta Gigante 42c, 34010 Sgonico, Trieste, Italy.*

*Fax: 0039 040 327521, e-mail: dgei@ogs.trieste.it*

*† Institute of Rock Structure and Mechanics,*

*Czech Academy of Sciences*

*V Holesovickach 41, Prague 8, 18200, Czech Republic*

*‡ Department of Earth Sciences,*

*University of Trieste*

*via Weiss, 4 - 34127, Trieste, Italy.*

(January 31, 2011)

Running head: **Vertical transverse isotropy from microseismic data**

## ABSTRACT

Microseismic data recorded by surface monitoring arrays can be used to estimate the effective anisotropic parameters of the overburden and reservoir. In this study we use P-wave arrival-time inversion of picked arrival times for estimating the Thomsen parameter  $\delta$  and the anellipticity coefficient  $\eta$ . The inversion is using analytic equation of P-wave arrival times as a function of offset in a homogeneous media with a vertical axis of symmetry.

In this study we analyze the sensitivity of the methodology to picking noise and uncertainties in the P-wave vertical velocity and source depth by inversion of synthetic arrival times. We also analyze the effect of increasing the maximum offset to source depth ratio and the number of receivers per line of the monitoring array. Long offsets effectively improve the estimation of  $\delta$  and  $\eta$  from noisy arrival times, as well as an high number of receivers per line, if we know the P-wave vertical velocity and source depth accurately. However, increasing the maximum offset to source depth ratio increases the inaccuracy of the estimated anisotropic parameters if we do not know the correct value of the P-wave vertical velocity or source depth. Such inaccuracy cannot be detected from the results of this inversion technique.

We also apply this P-wave arrival time inversion to field data acquired during the hydraulic fracturing of a gas shale reservoir and compare the results with anisotropic parameters estimated from synthetic arrival times computed with an isotropic layered medium. The effective anisotropy observed from the inversion of the field data is partially due to intrinsic anisotropic properties of the reservoir and/or of the overburden.

This study emphasizes the importance of using accurate values of vertical velocity and source depth in P-wave arrival time inversion for anisotropic parameters estimation and gives useful suggestions for designing microseismic monitoring arrays.

## INTRODUCTION

Elastic media, where seismic velocities depend on the direction of wave propagation at some physical points, are called anisotropic (e.g. Grechka (2009)). Most crustal rocks are found experimentally to be anisotropic. Anisotropy in sedimentary rock sequences may be caused by preferred orientation of anisotropic mineral grains (such as in a massive shale formation), preferred orientation of the shapes of isotropic minerals (such as flat-lying platelets), preferred orientation of cracks or thin bedding of isotropic or anisotropic layers (Thomsen, 1986). Transversely isotropic medium with vertical axis of symmetry (VTI) is believed to be the most common anisotropic model for sedimentary basins. Such a model is also called polar anisotropy (Thomsen, 2002). In this study we consider homogeneous VTI media which are equivalent (in traveltimes) to arbitrary complex 1D media of isotropic or VTI layers (Backus (1962), Grechka and Tsvankin (1998)).

Conventional processing of seismic data is based on the assumption of a subsurface made of isotropic homogeneous layers. However, especially in presence of shales, ignoring the contribution of the anisotropy to the normal moveout (NMO) velocity leads to mis-ties in time-to-depth conversion (e.g. Banik (1984), Alkhalifah et al. (1996), Sarkar and Tsvankin (2006)). Not only velocity analysis, but practically all other conventional seismic processing and interpretation techniques become inaccurate if the medium is anisotropic (Lynn et al. (1991), Tsvankin and Thomsen (1995), Alkhalifah and Larner (1994), Tsvankin (1995)).

A simple methodology to estimate effective anisotropic parameters from long-offset seismic data is the inversion of P-wave traveltime. VTI media are characterized by non-hyperbolic reflection moveout, more significant in large-offset arrivals for P- and SV-waves (rigorously we should call the fastest wave quasi-P-wave and slower waves polarized in

a vertical and horizontal plane quasi-SV-waves and quasi-SH-waves, respectively, but in VTI media quasi-SV-wave and quasi-SH-waves remain separated and thus we can use the same terminology as in isotropic media). Non-hyperbolicity of the moveout can also be related to vertical and lateral heterogeneity and reflectors curvature (Fomel and Grechka (1997)). This technique, widely used for active seismic (Tsvankin and Thomsen (1994), Alkhalifah and Tsvankin (1995), Alkhalifah and Tsvankin (1995), Grechka and Tsvankin (1998) ), can be efficiently applied also to microseismic data analysis. Although microseismic events generate also strong S-waves, the analysis of P-waves is simpler (as we can unambiguously pick the first arrival) and P-waves are less attenuated. Thus this study will focus on P-waves only.

Hydraulic fracture stimulation (fracking) is a commonly used technique to enhance hydrocarbon recovery by increasing the reservoir permeability. These stimulations consist of injection of high pressure fluids in rock formation. Such injections induce microseismic events, that are monitored to optimize hydraulic fracturing. A star-shaped array of surface (or near-surface) geophones can be used to monitor the induced microseismicity. Chambers et al. (2010b) test the ability to detect microseismic event with surface star-like array by location of several perforation shots in isotropic layered media. Anisotropic models are mostly derived from S-wave splitting from downhole data (for an overview see Verdon et al. (2009)) or calibration shots (e.g. Bulant et al. (2007)). Application of isotropic velocity model to surface monitoring of induced microseismicity is discussed in an application to data from Valhall by Chambers et al. (2010a). In their study only previously built (from active seismic monitoring) isotropic model is used while this study investigates possibility of building an effective anisotropic model. The monitoring of induced seismicity differs from active seismic by having more unknowns. The origin time is obviously not known

for microseismic events and often even for perforation shots. The locations of perforation shots are known with a limited precision, which depends on the accuracy of a well-deviation survey (Bulant et al. (2007)). A velocity model is usually calibrated from seismic signals of perforation shots at known positions along the treatment well.

In this study, we investigate the feasibility of inversion of the effective anisotropy parameters assuming a VTI model of the subsurface and its sensitivity to picking errors, uncertainties in the P-wave vertical velocity and source location. We also show results of the application of the P-wave arrival times inversion to four perforation shots in a gas shale reservoir as an example of a practical velocity model calibration.

## **P-WAVE TRAVELTIME INVERSION FOR HOMOGENEOUS TRANSVERSELY ISOTROPIC (TI) MEDIA**

Traditionally, inversion of P-wave traveltimes has been developed for active seismic applications (Tsvankin and Thomsen (1994), Alkhalifah and Tsvankin (1995), Alkhalifah and Tsvankin (1995), Grechka and Tsvankin (1998)). Considering the Pythagorean theorem, the traveltimes of direct P-wave arrival (from a subsurface source) for a single horizontal homogeneous isotropic layer is given by

$$t(x)^2 = t(0)^2 + x^2/V_{NMO}^2, \tag{1}$$

where  $t(0)$  is the zero offset one-way traveltimes,  $x$  is the offset, i.e. horizontal distance from the epicenter, and  $V_{NMO}$  is the normal moveout velocity, being the P-wave velocity of the isotropic medium (Figure 1). The moveout traveltimes described by equation 1 is hyperbolic.

Let's consider a single horizontal homogeneous transversely anisotropic layer with a vertical symmetry axis (VTI). In the small offset approximation equation 1 still holds, but

$$V_{NMO} = V_{P0}(1 + 2\delta)^{1/2}, \quad (2)$$

where  $V_{P0}$  is the P-wave vertical velocity (along the symmetry axis) and  $\delta$  is one of the Thomsen parameters (Thomsen, 1986). In small offsets the moveout is still hyperbolic but  $V_{NMO}$  is not the vertical nor the horizontal P-wave velocity of the horizontal medium.

Alkhalifah and Tsvankin (1995) showed that in laterally homogeneous VTI media the traveltimes of qP-waves depend mainly on the zero-dip normal-moveout velocity  $V_{NMO}$  and the anellipticity parameter  $\eta$ , controlling the nonhyperbolic moveout,

$$\eta = \frac{\epsilon - \delta}{1 + 2\delta}, \quad (3)$$

where  $\epsilon$  is one of the is one of the Thomsen parameters whose value in VTI media is close to the fractional difference between the horizontal and vertical P-wave velocities (Thomsen, 1986).

Alkhalifah and Tsvankin (1995) modified a three term Taylor series expansion of the moveout given by Tsvankin and Thomsen (1994) as

$$t^2(x) = t^2(0) + \frac{x^2}{V_{NMO}^2} - \frac{2\eta x^4}{V_{NMO}^2[t^2(0)V_{NMO}^2 + (1 + 2\eta)x^2]}, \quad (4)$$

where  $V_{NMO}$  is given by equation 2. The coefficient of the  $x^4$  is modified to fit horizontal velocity. This moveout equation is suitable for anisotropic parameter inversion from P-wave traveltimes in the large offset approximation. This equation can be used to invert arrival times from microseismic events (or perforation or calibration shots). Arrival times can be inverted in a non-linear iterative inversion minimizing the residuals between observed and synthetic traveltimes. This inversion uses as input arrival times  $t_A(x)$  determined along various offsets. These arrival times constrain traveltimes  $t(x)$  in equation 4 with additional unknown - origin time  $t_0$  as

$$t(x) = t_A(x) - t_0. \quad (5)$$

Thus to invert VTI parameters ( $\delta$  and  $\eta$ ) we need to either know or invert origin time  $t_0$ , vertical P-wave velocity  $V_{P0}$  and depth of the source (which determines the one-wave vertical traveltime  $t(0)$ ). Without a restriction on generality we assume that the horizontal position of the source is either known with sufficient accuracy (perforation shots) or determined from symmetry of the moveout, independently of the velocity model calibration.

## SYNTHETIC DATA

In this section we will describe synthetic dataset used in this study. The synthetic dataset mimics real dataset discussed in the section devoted to field data analysis. Here we investigate synthetic arrival times for homogeneous anisotropic media as they are equivalent to the layered model; such model is appropriate for majority of fractured shale basins. Figure 1 shows a vertical cross-section through the synthetic passive seismic monitoring

experiment of this study. The microseismic source is located at depth  $z_S$  and the receiver at an offset  $x$ .  $t(x)$  is the travelttime at offset  $x$  and  $t(0)$  is the one-way vertical travelttime. To compute synthetic arrival times and perform the P-wave arrival time inversion, receivers are arranged in 8 regularly spaced lines ( $45^\circ$  spacing) radiating from a central point, in a star like pattern. The source is located in the center of the star at 2100 m depth as illustrated in Figure 2. The coordinates of the source are  $x_S = 3350$  m,  $y_S = 3350$  m and  $z_S = 2100$  m. The effective vertical velocity  $V_{P0}^{\text{true}}$  is 2906 m/s and the anisotropic parameters are  $\delta = 0.1$  and  $\eta = 0.1$ . We chose  $\delta$  to be similar to  $\eta$  as we wish to study the relative sensitivity of these parameters in this configuration. From the computed travelttimes we subtract 0.5 s, corresponding to the origin time  $t_0 = -0.5$  s.

The travelttimes are computed with equation 4, meaning we use the same equation to produce and invert travelttimes. We have also used alternative computations of travelttimes (e.g. full waveform modeling (Carcione (2007)) and picking, and travelttimes computed with equations listed in Bulant et al. (2007)) and obtained very similar results, therefore we assume that this choice does not affect our conclusions. To simulate picking noise we perturb synthetic arrival times with Gaussian noise with zero mean and increasing values of standard deviation  $\sigma_n$ , from 0 to 4 ms. The standard deviation of the Gaussian noise is given by

$$\sigma_n = \sqrt{\frac{\sum_{i=1}^N n_i^2}{N}}, \quad (6)$$

where  $n_i$  is noise added to the the travelttimes. And analogously the RMS of residuals (either residuals from synthetic or real datasets) is

$$RMS = \sqrt{\frac{\sum_{i=1}^N (t_i^{\text{data}} - t_i^{\text{synth}})^2}{N}}, \quad (7)$$

where  $t_i^{\text{data}}$  are input arrival times and  $t_i^{\text{synth}}$  are computed arrival times with equation 4 and the inverted parameters.

Figure 3 shows an example of synthetic traveltimes for one line of the star-pattern surface array without noise and with Gaussian noise ( $\sigma_n = 4$  ms).

## SENSITIVITY ANALYSIS OF P-WAVE TRAVELTIME INVERSION

In the following inversion tests we will invert for anisotropic parameters ( $\delta$  and  $\eta$ ) and origin time  $t_0$ . As input parameters we will use arrival times with variable noise levels, the vertical P-wave velocity  $V_{P0}$ , and the source location ( $x_S, y_S, z_S$ ). We will investigate the sensitivity of the inverted parameters on input parameters, in particular the source depth and vertical P-wave velocity. We consider the horizontal coordinates of the source ( $x_S$  and  $y_S$ ) as known parameters, as they can be robustly inverted in VTI media. We do not invert more than three parameters ( $\delta, \eta$  and  $t_0$ ) as equation 4 shows that only three coefficients of the Taylor expansion can be determined independently. This is analogous to inversion described in Bulant et al. (2007) where also only three parameters can be determined independently. In our case we chose origin time and anisotropic for practical reason to mimic an inversion of perforation data with unknown origin time. However, if the origin time is known we can invert vertical velocity instead.

## Sensitivity to picking noise

In principle, once the VTI character of the subsoil has been ascertained, the inversion of P-wave arrival times can be performed for a single seismic line, e.g. a single arm of the star array. However, in presence of picking noise, the large number of arrival times (from larger number of receivers) provides better statistical sampling resulting in more precise estimate of the anisotropic parameters  $\delta$  and  $\eta$ . Figure 4 shows the results of 100 inversions, each of them characterized by a different realization of the Gaussian noise ( $\sigma_n = 4$  ms). The maximum offset to source depth ratio (MO/SD) is 1.5, the receivers interval is 16 m and the number of receivers per line is 200. Triangles and circles show inverted  $\delta$  and  $\eta$  using the 8 arms star array and line 1 of receivers (Figure 3), respectively. The two anisotropic parameters are characterized by a linear trend as values of  $\delta$  and  $\eta$  trade-off with each other. Inversions of dataset from the star array result in tighter cluster than inversions of the data from single line 1, both accurately centered on the true (input) values. Consequently hereafter we perform inversions with the star array geometry.

Figure 5 shows the inverted  $\delta$  (a) and  $\eta$  (b) with different levels of the Gaussian noise ( $\sigma_n$ ) in the synthetic arrival times. Figure 5 (c) and (d) show inverted origin times  $t_0$  and the root mean square of time residuals (RMS). The maximum offset to source depth ratio (MO/SD) is 1.5, the receiver interval is 16 m and the number of receivers per line is 200. For each noise level ( $\sigma_n$ ) we compute 100 realizations. Inaccuracies in the estimated anisotropic parameters are proportional to the picking noise and  $\eta$  is more sensitive than  $\delta$  to the noise level.  $t_0$  is little affected by the picking noise. The root mean square of time residuals RMS (Figure 5 (d)), has the same value of  $\sigma_n$ ; thus we may use measured RMS values in real dataset as an estimate of the noise in picked arrival times.

Figure 6 shows the standard deviation of  $\delta$  (a) and  $\eta$  (b) vs the maximum offset to source depth ratio (MO/SD) with  $\sigma_n$  of 4 ms. For each MO/SD value, the curves represent the standard deviation of 100 estimated anisotropic parameters, corresponding to 100 noise realizations in the synthetic arrival times. Figure 6 shows 3 curves in each plot. To obtain the curves (1), we increase the offset by adding receivers to each arm of the star array; the receiver interval is constant (25 m) and the receivers number varies between 63 (MO/SD = 0.75) and 168 (MO/SD = 2). The curves (2) are computed by keeping constant the number of receivers per line (100) and increasing the receiver interval from 16 m (MO/SD = 0.75) to 42 m (MO/SD = 2). The curves (3) use 200 receivers per line and receiver intervals from 8 m (MO/SD = 0.75) to 21 m (MO/SD = 2). The standard deviation of the inverted  $\delta$  and  $\eta$  decreases as MO/SD increases. The fastest decrease of the error is for MO/SD smaller than 1:1 and the improvement to the inverted anisotropic parameters from offsets larger than 1.5 source depth is negligible. The larger number of receivers per line provides a better estimate of anisotropic parameters simply by the means of better statistical sampling of noise (similar to the test of Figure 4).

This is also shown in Figure 7 by plotting the standard deviation of  $\delta$  (a) and  $\eta$  (b) as a function of the number of receivers per line (nr) for a fixed MO/SD. For each value nr, we show standard deviations of  $\delta$  and  $\eta$  resulting from 100 noise realization of arrival times. MO/SD is 1.5 and arrival times are affected by picking noise ( $\sigma_n$  of the normal distribution is 4 ms). The maximum offset is kept constant and increasing the number of receivers reduces the receiver spacing. The estimated values of  $\delta$  and  $\eta$  dramatically improves as more receivers are added to each arm of the star array up to 200 receivers corresponding to a receiver interval of 15 m. Note that the uncertainty reduction approximately fall off as  $\frac{1}{\sqrt{N}}$  where N is the number of receivers.

## Sensitivity to P-wave vertical velocity

To study the sensitivity of this P-wave arrival time inversion technique to input value of the P-wave velocity in the vertical direction ( $V_{P0}$ ) we perform arrival time inversions considering 7 different velocity values, ranging from -10 to +10% of the actual value  $V_{P0}^{\text{true}}$ . Synthetic traveltimes are computed with the actual values of the P-wave vertical velocity  $V_{P0}^{\text{true}}$  but they are inverted considering uncorrect values of  $V_{P0}$ .

Figure 8 shows inverted  $\delta$  (a) and  $\eta$  (b), origin time  $t_0$  (c) and RMS of time residuals (d) as function of assumed input P-wave vertical velocity  $V_{P0}$ . For each value of the P-wave vertical velocity we perform 100 inversions, corresponding to 100 noise realizations in the synthetic arrival times. The standard deviation of the Gaussian noise is 4 ms. The maximum offset to source depth ratio is 1.5 and the number of receivers per arm is 200. Each circle in the Figures 8 (a)-(d) represents the result of one of the 100 performed inversions. For P-wave vertical velocities differing from the actual value ( $V_{P0} = 2906$  m/s) the estimated  $\delta$  (a) and  $\eta$  (b) reveal a systematic bias increasing almost linearly with actual difference between the correct and input vertical velocity. However, scatter (or standard deviation) of the inverted anisotropic parameters remains approximately constant and is dependent on the level of noise in the arrival times (see the plot 8 (d)). The bias, also known as accuracy, of the two inverted anisotropic parameters is proportional to  $|V_{P0} - V_{P0}^{\text{true}}|$ . The scatter, also known as precision, depends only on level of noise in arrival times. As the noise level was kept constant in this test the inverted  $\delta$  and  $\eta$  show a constant scatter (uncertainty) for all the  $V_{P0}$  values. Origin time  $t_0$ , shown in Figure 8 (c) is not affected by the Gaussian noise, but it is dependent on the input P-wave vertical velocity. The RMS of time residuals (Figure 8 (d)) equals the noise level ( $\sigma_n$ ) but it is unaffected by

$V_{P0}$ . The presence of picking noise in the input arrival times can be inferred from the root mean square of the time residuals. Instead, inaccurate values of the input P-wave vertical velocity cause proportional inaccuracies in the estimated anisotropic parameters that cannot be detected from the results of the inversion RMS or any other result.

Figure 9 (a) and (b) shows the means (solid lines) and standard deviations (shaded areas) of 100 inverted  $\delta$  and  $\eta$  on the maximum offset to source depth ratio (MO/SD). We show three dependencies for three different input vertical velocities:  $V_{P0} = 0.9V_{P0}^{\text{true}}$ ,  $V_{P0} = V_{P0}^{\text{true}}$  and  $V_{P0} = 1.1V_{P0}^{\text{true}}$ . The input arrival times are perturbed with Gaussian noise ( $\sigma_n = 4$  ms). These are mean values of 100 realizations of randomly distributed Gaussian noise in the inverted picking noise. They represent the accuracy of the inversion method as a function of MO/SD and  $V_{P0}$ . The standard deviations  $\sigma_\delta$  and  $\sigma_\eta$  (shaded area) for the increasing maximum offset to source depth ratio are related to the Gaussian noise in the arrival times. The surprising result is increasing bias (inaccuracy) for  $\eta$  with increasing maximum offset for  $V_{P0} \neq V_{P0}^{\text{true}}$ . There are two sources of uncertainty in the estimated parameters: the lack of accuracy, highlighted by the means and related to the uncorrect value of  $V_{P0}$ , and the lack of precision, highlighted by the standard deviations, and due to the picking noise. For the Thomsen parameter  $\delta$  both the accuracy and precision improve with increasing the MO/SD. The accuracy of the anellipticity coefficient  $\eta$  strongly decreases as the maximum offset increases, and the precision slightly increases.

### Sensitivity to source depth

Similarly to the test used for the sensitivity analysis to the P-wave vertical velocity, we invert arrival times perturbed with white Gaussian noise ( $\sigma_n = 4$  ms) with various

source depth values  $z'_S$  ranging from  $0.95z_S$  to  $1.05z_S$ , where  $z_S$  is the actual source depth used to compute the arrival times.

Figure 10 shows  $\delta$  (a) and  $\eta$  (b), origin time  $t_0$  (c) and RMS of time residuals (d) as a function of  $z'_S$ . For each value  $z'_S$  we perform 100 inversions, corresponding to 100 noise realizations. The standard deviation of the Gaussian noise is 4 ms. The maximum offset to source depth ratio is 1.5 and the number of receivers in each line is 200. For source depths different from the actual value ( $z_S = 2100$  m) the inverted  $\delta$  and  $\eta$  are characterized by a systematic error proportional to  $|z'_S - z_S|$ .  $z'_S$  affects the accuracy, but not the precision, of the inversion results. The precision is again controlled by noise in the arrival times only, as the scatter remains constant in Figures 10 (a), (b) and (d). The inverted origin times (panel (c)) are not affected by the Gaussian noise but they strongly depend on the source depth.

Figure 11 shows the means (solid lines) and standard deviations (shaded areas) of  $\delta$  (a) and  $\eta$  (b) as a function of the source to depth ratio (MO/SD); three values of source depths were tested:  $z'_S = 0.95z_S$ ,  $z'_S = z_S$  and  $z'_S = 1.05z_S$ . Accuracy of the inversion of both the anisotropic parameters decreases with increasing offset. This can be understood from the fact that VTI anisotropy mainly affects horizontal traveltimes. Thus as the offset increases the ray paths become more horizontal and erroneous depth is compensated by stronger VTI parameters. The precision of the inversion method, emphasized by the standard deviations  $\sigma_\delta$  and  $\sigma_\eta$  strongly increases with MO/SD (the shaded areas narrows with increasing MO/SD), giving incorrect impression of more accurate results.

Similarly to the results of the P-wave vertical velocity test, the noise level in arrival times can be gathered from the root mean square of the time residuals. Incorrect source

depth causes inaccuracy in the estimated  $\delta$  and  $\eta$  and this inaccuracy increases with greater maximum offsets. Such inaccuracies do not show in by any output parameter of the inversion.

## FIELD DATA

A microseismic monitoring was performed by Microseismic Inc. during the hydraulic fracturing of a gas shale reservoir located in North America operated by Newfield Exploration Mid-Continent Inc.. They used a 10 lines *Fracstar*® array (Figure 12) with 1C geophones located at the Earth surface. The number of receivers per arm varies between 54 (line 4) and 122 (lines 2 and 10) and the average receiver distance is 23 m.

The productive formation is accessed by perforating the casing at reservoir depth. Such shots are used for velocity model calibration (both in downhole and surface monitoring) and we investigate the feasibility of inversion of anisotropic parameters for an homogeneous VTI medium. As the tests on synthetic datasets in previous sections revealed, the inverted anisotropic parameters are strongly dependent on correct depth of a microseismic event. The depth of induced microseismic events is unknown, therefore we use only perforation shots whose position is known with a high accuracy (less than 2% error as discussed in Bulant et al. (2007)).

We invert arrival times from 4 perforation shots fired in the horizontal section of one of the four deviated wells piercing the reservoir. All of the shots belong to the same stage with a horizontal shot separation of 37 m; vertical separation of shots is negligible. Perforation shots coordinates are given in Table 1 ( $x_S, y_S, z_S$ ). Figure 12 shows the manually picked and interpolated arrival times for the perforation shot 1. Microseismic data from the north-western part of the array are noisy and we could not pick the first

arrivals. Figure 13 shows an example of seismic sections relative to shot 1. We apply a bandpass frequency filter with corner frequencies 6, 12, 60, 70 Hz. The 1D vertical velocity profile derived from 3D active seismic over the reservoir is shown in Figure 14. In order to apply the P-wave traveltime inversion for homogenous-anisotropic media to this dataset, we compute the effective vertical velocity at the source depth: for a given depth of a seismic source, the effective velocity is the P-wave velocity of an equivalent homogeneous medium giving the same zero-offset traveltime as the layered medium. Figure 14 shows the 1D P-wave vertical profile (continuous lines) and the effective vertical velocity (dashed curve). The effective velocity at the depth of perforation shots is  $V_{P0} = 2906$  m/s. Figure 15 shows the time residuals of perforation Shot 1 interpolated in a map view plot (a) and as a function of offset (b). The results of the inversions of picked arrival times from the four perforation shots are given in Table 2. The  $\delta$  and  $\eta$  are significantly high, indicating anisotropic medium. Table 2 shows a good consistency among the estimated anisotropic parameters of the four perforation shots. Shot 4 gives a slightly higher  $\delta$  and a lower  $\eta$  with respect the other shots. The Shot 4 was least constrained as we could pick only arrivals from lines (1), (2), (3), (10) and part of (9) (see Figure 12 for line number reference). Finally considering the resulting RMS and comparing this RMS to the test of Figure 4 we can see that the scatter of the inverted anisotropic parameters is very consistent and even the 'error' of inverted parameters from the Shot 4 is consistent with the  $\delta - \eta$  trade-off observed in the test on synthetic dataset.

Non-hyperbolicity of moveout can be also caused by vertical and lateral heterogeneity (Backus (1962), Fomel and Grechka (1997)). Inversions of arrival times in isotropic layered media can result in apparent anisotropy. To estimate the influence of layering on the above inverted effective anisotropy we compute and invert synthetic arrival times for a layered

isotropic medium. We consider a horizontally layered model suitable for this dataset with the P-wave velocity profile shown in Figure 14 (continuous line). We compute synthetic traveltimes in the isotropic layered model and add Gaussian noise with zero mean and  $\sigma_n = 4$  ms. Figure 16 shows the time residuals from the inversion of synthetic arrival times computed with the same geometry of this dataset (see Figure 15). Results of the P-wave arrival time inversion of these data are given in Table 2 (Isotropic). The isotropic layers suitable for this region seem to cause only about 50% of the effective anisotropy indicating that the media is also anisotropic.

## CONCLUSIONS

In this study, we investigate reservoir characterization from an array of sensors deployed at the earth's surface with a star geometry, to monitor hydraulic stimulations. We explore the sensitivity of the P-wave arrival time inversion to picking errors, uncertainties in the P-wave vertical velocity and source location, and specifically their influence on the estimated Thomsen parameter  $\delta$  and the anellipticity coefficient  $\eta$ . We compute synthetic traveltimes, add randomly distributed Gaussian noise and perform inversions, considering perturbations of the vertical P-wave velocity, and source depth.

Inversions of arrival times with Gaussian noise affects precision of resulting anisotropic parameters  $\delta$  and  $\eta$ , whereas the origin time is estimated accurately. The parameter  $\delta$  is slightly less sensitive to the noise than  $\eta$  for the geometry considered in this study. The root mean square of time residuals has the same value of the standard deviation of the Gaussian noise; thus we may use the measured RMS values in real datasets as an estimate of the noise level in arrival times. Long offsets of the lines forming the star-pattern array improves the anisotropic parameters estimation, most effectively up to 1.5 of the maximum

offset to depth ratio. Increasing the number of receivers per line of the star array also increases the precision of the resulting anisotropic parameters as we improve statistical sampling.

Uncertainties in the vertical velocity strongly influence the origin time, the anisotropic parameters  $\delta$  and  $\eta$  resulting from the inversion procedure, revealing a systematic bias increasing almost linearly with actual difference between the correct and input velocity. Scatter (or standard deviation) of the inverted anisotropic parameters remains approximately constant for a given maximum offset to source depth ratio, and is dependent on the level of noise in the arrival times. Again, the root mean square of time residuals approximately equals the noise level and it is unaffected by the input vertical velocity. Increasing the maximum offset to source depth ratio slightly improves the estimation of  $\delta$  but, surprisingly, increases the bias (inaccuracy) of  $\eta$ . We obtain similar results studying the influence of uncertainties of the source depth on the estimated anisotropic parameters. For any given maximum offset to source depth ratio, the difference between the correct and input source depth affects the accuracy of the inversion results. Their precision is again controlled by noise level in the arrival times only, as the scatter remains constant for varying the source depth. Increasing the maximum offset decreases the accuracy of the inversion of both the estimated  $\delta$  and  $\eta$ . Instead, the precision of the inversion method increases, giving incorrect impression of more accurate results. Inaccurate values of the P-wave vertical velocity and source depth cause proportional inaccuracies in the estimated anisotropic parameters that cannot be detected from the results of this inversion. This emphasizes the importance of using accurate vertical velocity and source depth as inputs of the inversion.

We apply the P-wave arrival time inversion to four perforation shots recorded from a

microseismic monitoring. We have obtained consistent result from the four independent inversions resulting in approximately  $\delta=0.27$  and  $\eta=0.12$ . Furthermore, we also inverted arrival times computed with isotropic layered model suitable for this reservoir and obtained only approximately 50% strength of the anisotropy. Thus we conclude that the observed anisotropy is cause partially by intrinsic anisotropic properties of this formation.

### ACKNOWLEDGEMENTS

We are very grateful to Vladimir Grechka of Shell for guidance, suggestions and discussions. We are also grateful for a kind revision, advise and providing data to the Newfield Exploration Mid-Continent Inc., particularly to Jack Breig, Richard Parkes, Keith Willson and Michelle Langthorn. We also thank Microseismic Inc. for the data and support provided for the data management (including picking software); special thanks belong to Dave Abbott, Michael Thornton, Mike Mueller, Alejandro De La Peña and Peter Duncan.

## REFERENCES

- Alkhalifah, T., and K. Larner, 1994, Migration error in transversely isotropic media: Geophysics, **59**, 1405–1418.
- Alkhalifah, T., and I. Tsvankin, 1995, Velocity analysis for transversely isotropic media: Geophysics, **60**, 1550–1566.
- Alkhalifah, T., I. Tsvankin, K. Larner, and J. Toldi, 1996, Velocity analysis and imaging in transversely isotropic media: Methodology and a case study: The Leading Edge, **15**, 371–378.
- Backus, G. E., 1962, Long-wave elastic anisotropy produced by horizontal layering: J. Geophys. Res., **67**, 4427–4440.
- Banik, N. C., 1984, Velocity anisotropy of shales and depth estimation in the north sea basin: Geophysics, **49**, 1411–1419.
- Bulant, P., L. Eisner, I. Pšenčík, and J. L. Calvez, 2007, Importance of borehole deviation surveys for monitoring of hydraulic fracturing treatments: Geophysical Prospecting, **55**, 891–899.
- Carcione, J. M., 2007, Wave fields in real media. theory and numerical simulation of wave propagation in anisotropic, anelastic, porous and electromagnetic media.: Elsevier.
- Chambers, K., J. M. Kendall, and O. Barkved, 2010a, Investigation of induced microseismicity at valhall using the life of field seismic array: The Leading Edge, **29**, 290–295.
- Chambers, K., J. M. Kendall, S. Brandsberg-Dahl, and J. Rueda, 2010b, Testing the ability of surface arrays to monitor microseismic activity: Geophysical Prospecting, **58**, 821–830.
- Fomel, S., and V. Grechka, 1997, On nonhyperbolic reflection moveout in anisotropic media: Technical Report 92, Stanford Exploration Project,

[www.sepwww.stanford.edu/public/docs/sep92/sergey4.ps.gz](http://www.sepwww.stanford.edu/public/docs/sep92/sergey4.ps.gz).

- Grechka, V., 2009, Applications of seismic anisotropy in the oil and gas industry: EAGE.
- Grechka, V., and I. Tsvankin, 1998, Feasibility of nonhyperbolic moveout inversion in transversely isotropic media: *Geophysics*, **63**, 957–969.
- Lynn, W., A. Gonzalez, and S. MacKay, 1991, Where are the fault-plane reflections?: 61st Ann. Internat. Mtg., Soc. Exp. Geophys., Expanded Abstracts.
- Sarkar, D., and I. Tsvankin, 2006, Anisotropic migration velocity analysis: Application to a data set from west africa: *Geophysical Prospecting*, **54**, 575–587.
- Thomsen, L., 1986, Weak elastic anisotropy: *Geophysics*, **51**, 1954–1966.
- , 2002, Understanding seismic anisotropy, in exploration and exploitation: SEG.
- Tsvankin, I., 1995, Normal moveout from dipping reflectors in anisotropic media: *Geophysics*, **60**, 268–284.
- Tsvankin, I., and L. Thomsen, 1994, Nonhyperbolic reflection moveout in anisotropic media: *Geophysics*, **59**, 1290–1304.
- , 1995, Inversion of reflection traveltimes for transverse isotropy: *Geophysics*, **60**, 1095–1107.
- Verdon, J. P., J. M. Kendall, and A. Wüstefeld, 2009, Imaging fractures and sedimentary fabrics using shear wave splitting measurements made on passive seismic data: *Geophysical Journal International*, **179**, 1245–1254.

## TABLES

Table 1: Input parameters P-wave traveltimes inversions.

|        | $x_S$ (m) | $y_S$ (m) | $z_S$ (m) | $V_{P0}^{\text{true}}$ (m/s) |
|--------|-----------|-----------|-----------|------------------------------|
| Shot 1 | 2343      | 2410      | 2100      | 2906                         |
| Shot 2 | 2341      | 2517      | 2100      | 2906                         |
| Shot 3 | 2341      | 2552      | 2099      | 2906                         |
| Shot 4 | 2342      | 2590      | 2100      | 2906                         |

Table 2: Results of P-wave traveltimes inversions.

|           | $t_0$ (s) | $\delta$ | $\eta$  | RMS (ms) |
|-----------|-----------|----------|---------|----------|
| Shot 1    | - 0.256   | 0.1173   | 0.2734  | 4.0      |
| Shot 2    | 0.666     | 0.1207   | 0.2644  | 3.4      |
| Shot 3    | 0.433     | 0.1205   | 0.2763  | 3.3      |
| Shot 4    | - 0.118   | 0.1358   | 0.2223  | 4.4      |
| Isotropic | 0.001     | 0.0115   | 0.11537 | 4.3      |

## FIGURES

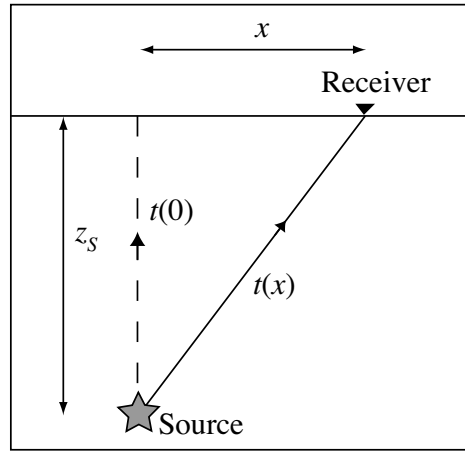


Figure 1: Schematic representation of a passive seismic monitoring experiment.

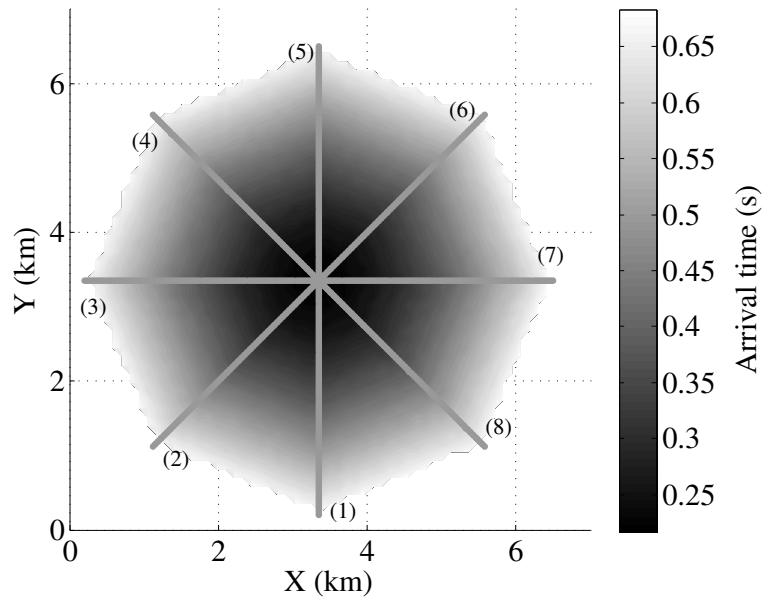


Figure 2: Arrival time contour over a plan view of a typical layout for surface array monitoring of hydraulic stimulation. The source is located in the center of the star. The gray lines represent the different arms of the star-pattern array.

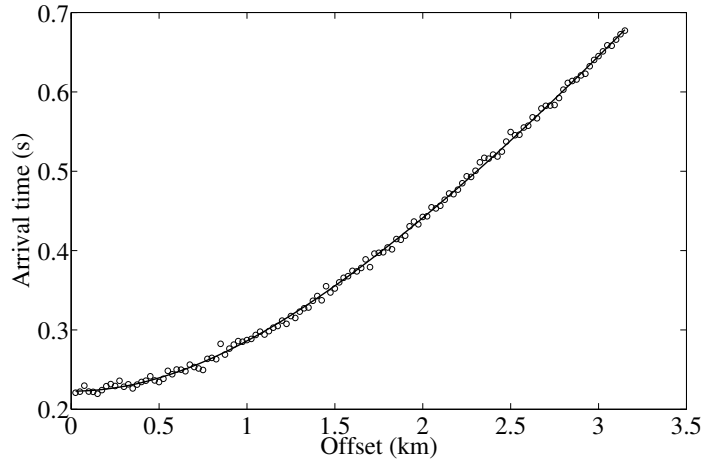


Figure 3: Example of synthetic traveltimes with (circles) and without (continuous line) Gaussian noise ( $\sigma_n = 4$  ms).

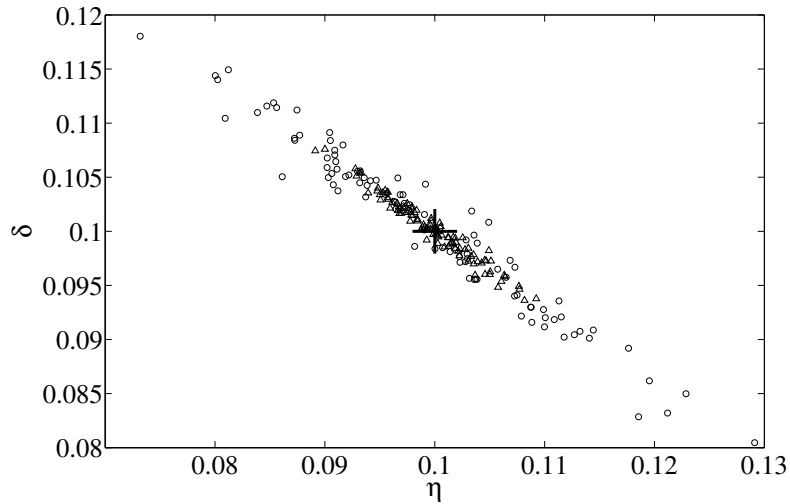


Figure 4:  $\delta$  versus  $\eta$  as results of inversions of traveltimes perturbed with 100 different realizations of Gaussian noise ( $\sigma_n = 4$  ms) . Triangles correspond inversions with the star geometry, while circles to inversions with a single line geometry. The cross gives the actual values of the anisotropic parameters ( $\delta = 0.1$  and  $\eta = 0.1$ ).

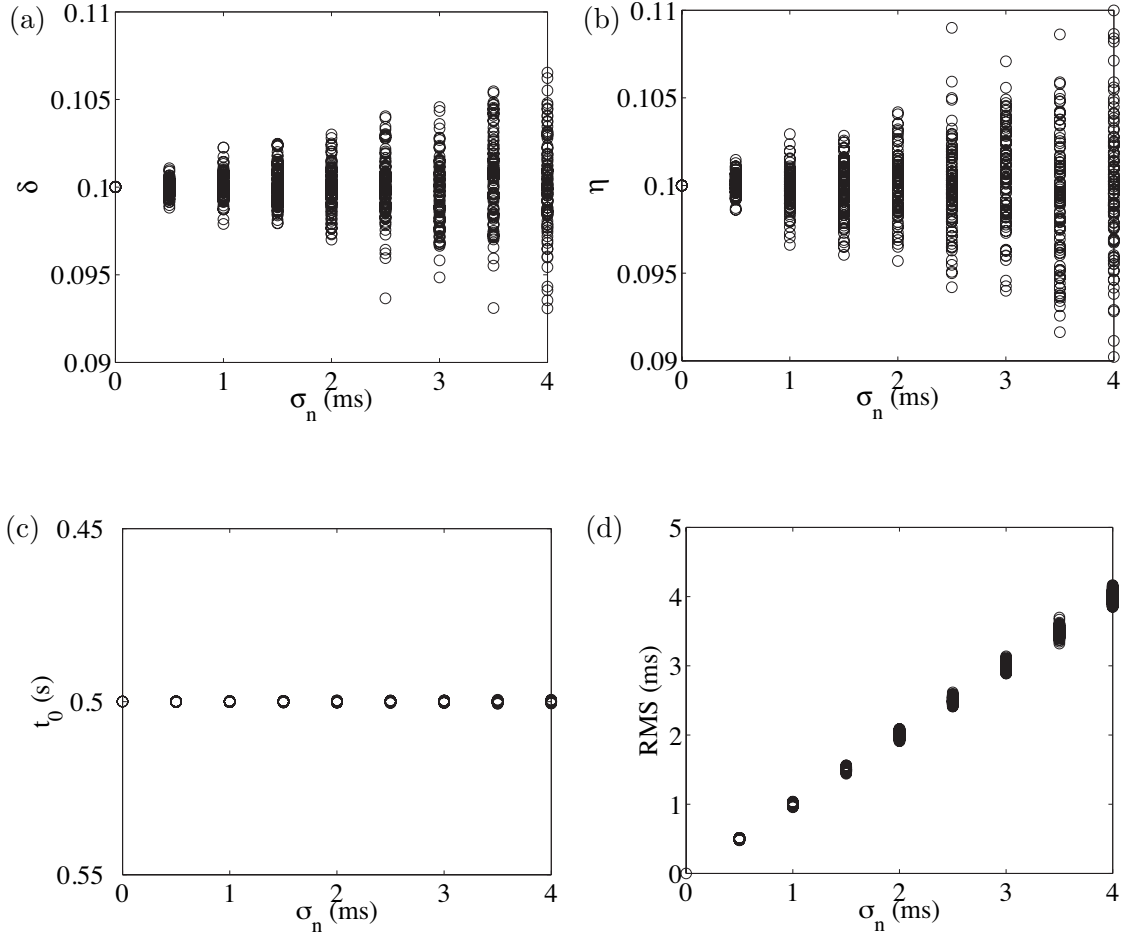


Figure 5: Estimated anisotropic parameter  $\delta$  (a),  $\eta$  (b), origin time  $t_0$  (c) and RMS of time residuals (d) for nine values of standard deviation of Gaussian noise ( $\sigma_n$ ). The maximum offset to source depth ratio (MO/SD) is 1.5, the receivers distance is 16 m and the number of receivers per line is 200.

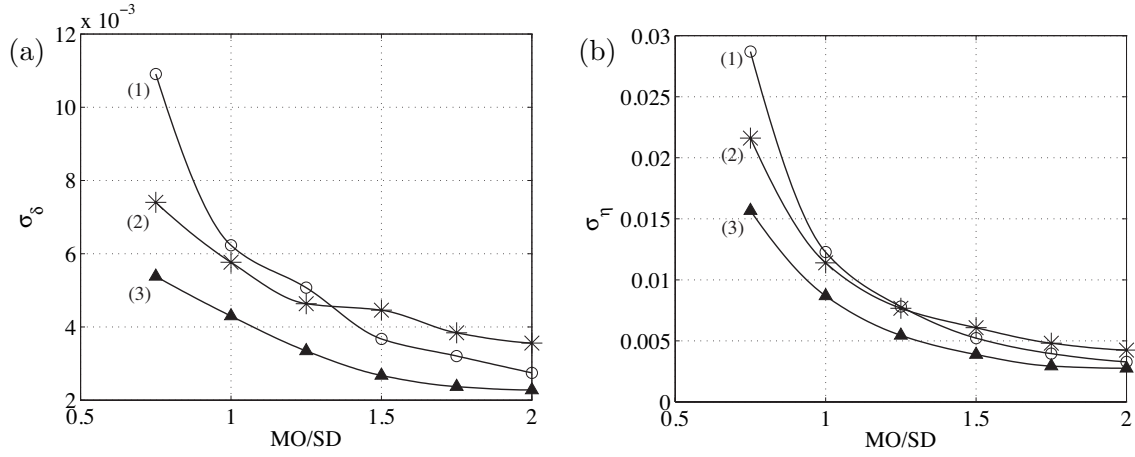


Figure 6: Standard deviation of 100 estimations of anisotropic parameter  $\delta$  (a) and  $\eta$  (b) vs maximum offset to source depth ratio (MO/SD). The standard deviation for the Gaussian noise perturbing the synthetic traveltimes is 4 ms. For curves (1) the maximum offset is increased by increasing the number of receivers in each line of the star array, from 63 (MO/SD = 0.75) to 168 (M)/SD = 2), whilst for curves (2) and (3) the arms are stretched increasing the receiver distance and keeping constant the number of receivers per line (100 for curve (2) and 200 for curve (3)).

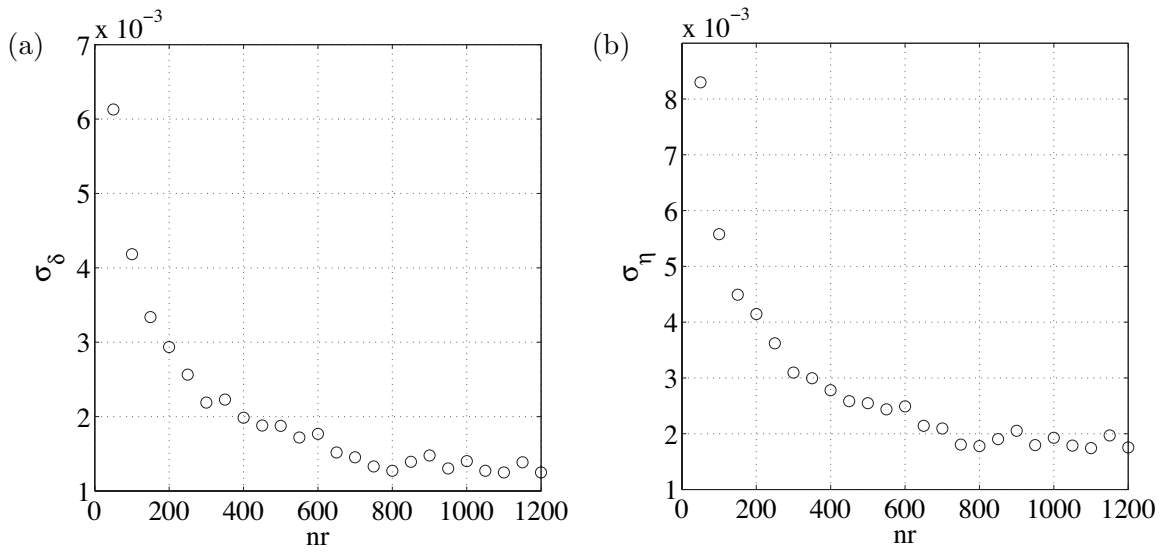


Figure 7: Standard deviation of the anisotropic parameter  $\delta$  (a) and the anellipticity coefficient  $\eta$  (b) vs the number of receivers per line (nr). Each circle is the standard deviation of 100 estimations corresponding to the same number of different noise realization. The maximum offset to source depth ratio is 1.5. The standard deviation for the Gaussian noise is 4 ms.

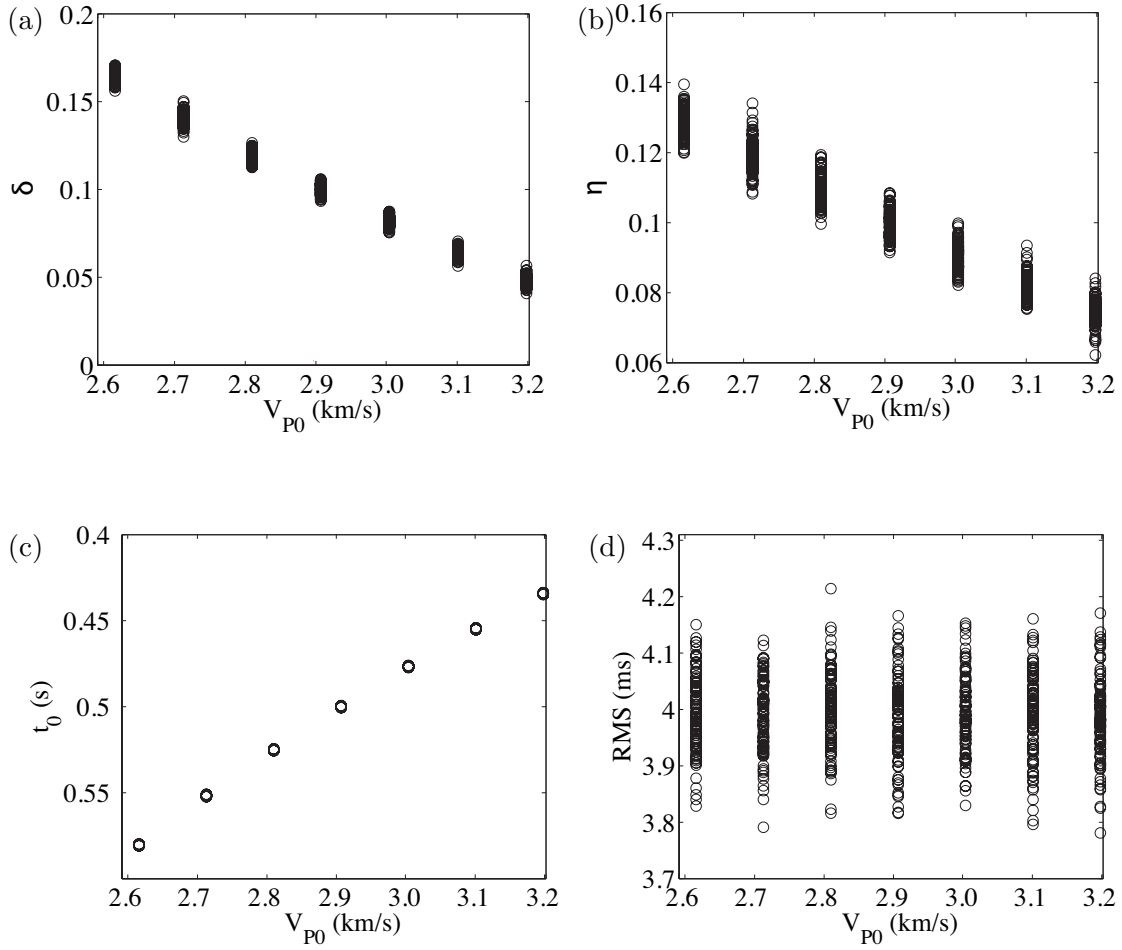


Figure 8:  $\delta$  (a),  $\eta$  (b), origin time  $t_0$  (c) and RMS of time residuals (d) vs P-wave vertical velocity. The maximum offset to source depth ratio is 1.5, the standard deviation for Gaussian noise is 4 ms and the number of receiver per line of the star array is 200.

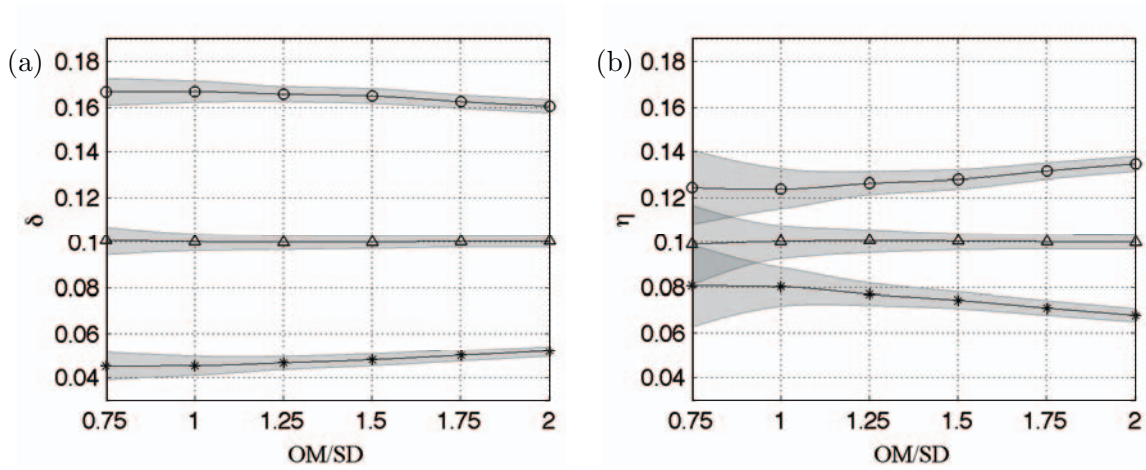


Figure 9: Means (solid lines) and standard deviations (shaded areas) of  $\delta$  (a) and  $\eta$  (b) vs offset to source depth ratio (MO/SD). We use  $V_{P0} = 0.9V_{P0}^{\text{true}}$  for data points represented by circles,  $V_{P0} = V_{P0}^{\text{true}}$  for triangles and  $V_{P0} = 1.1V_{P0}^{\text{true}}$  for asterisks. Standard deviation for Gaussian noise is 4 ms. Means and standard deviations are computed from the results of 100 inversions corresponding to the same number of noise realizations.

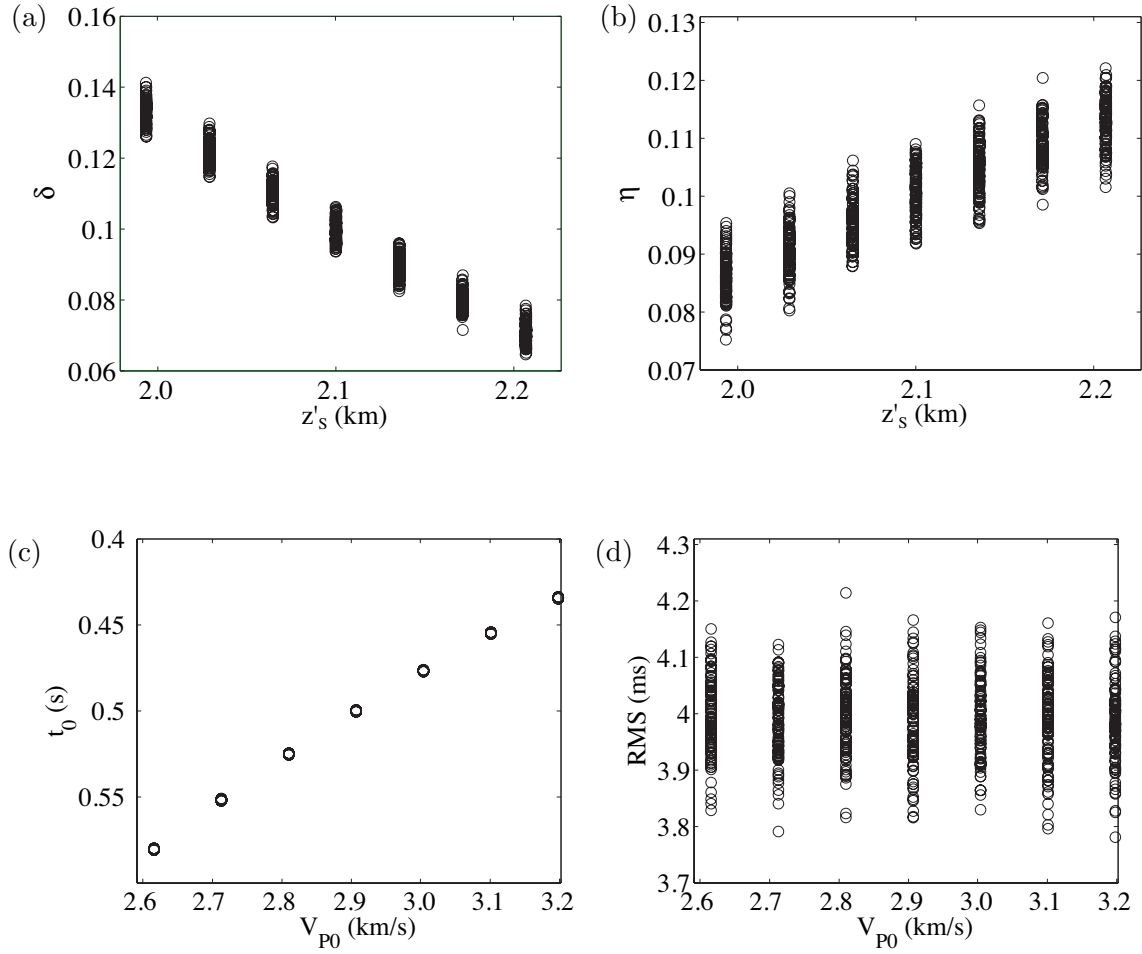


Figure 10:  $\delta$  (a),  $\eta$  (b), origin time  $t_0$  (c) and RMS of time residuals (d) vs source depth.

The maximum offset to source depth ratio is 1.5, the standard deviation for Gaussian noise is 4 ms and the number of receiver per line of the star array is 200.

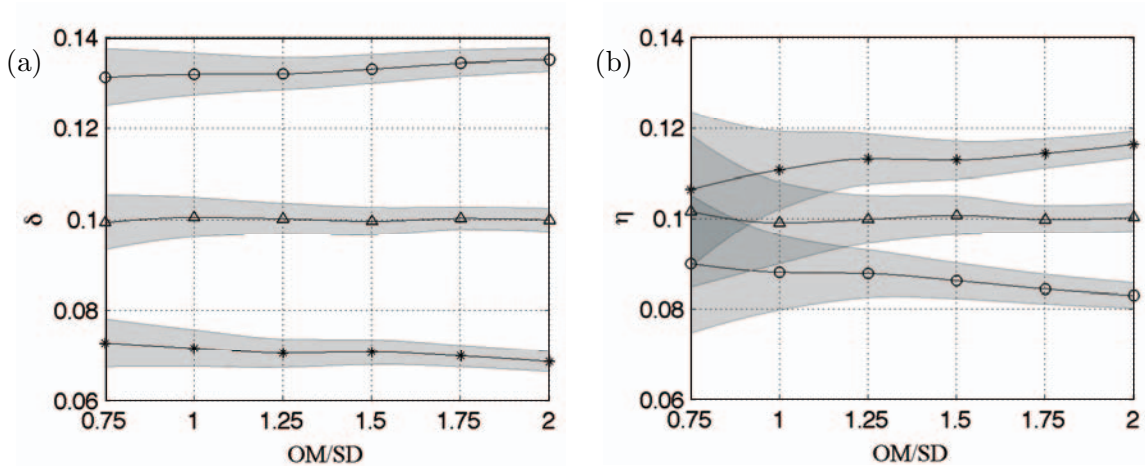


Figure 11: Means (solid lines) and standard deviations (shaded area) of  $\delta$  (a) and  $\eta$  (b) vs offset to source depth ratio (MO/SD). We use  $z'_S = 0.95z_S$  for data points represented by circles,  $z'_S = z_S$  for triangles and  $z'_S = 1.05z_S$  for asterisks. Standard deviation for Gaussian noise is 4 ms. Means and standard deviations are computed from the results of 100 inversions corresponding to the same number of noise realizations.

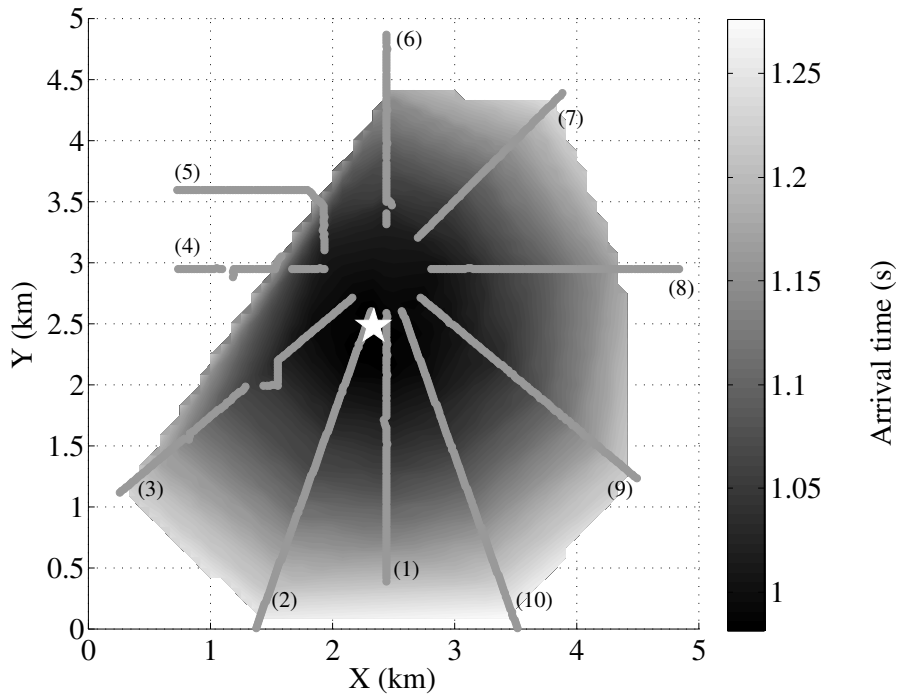


Figure 12: Contour plot showing the picked arrival times for the perforation shot 1. The straight gray, numbered lines represent the 10 seismic lines of the Fracstar. The white star is the source location.

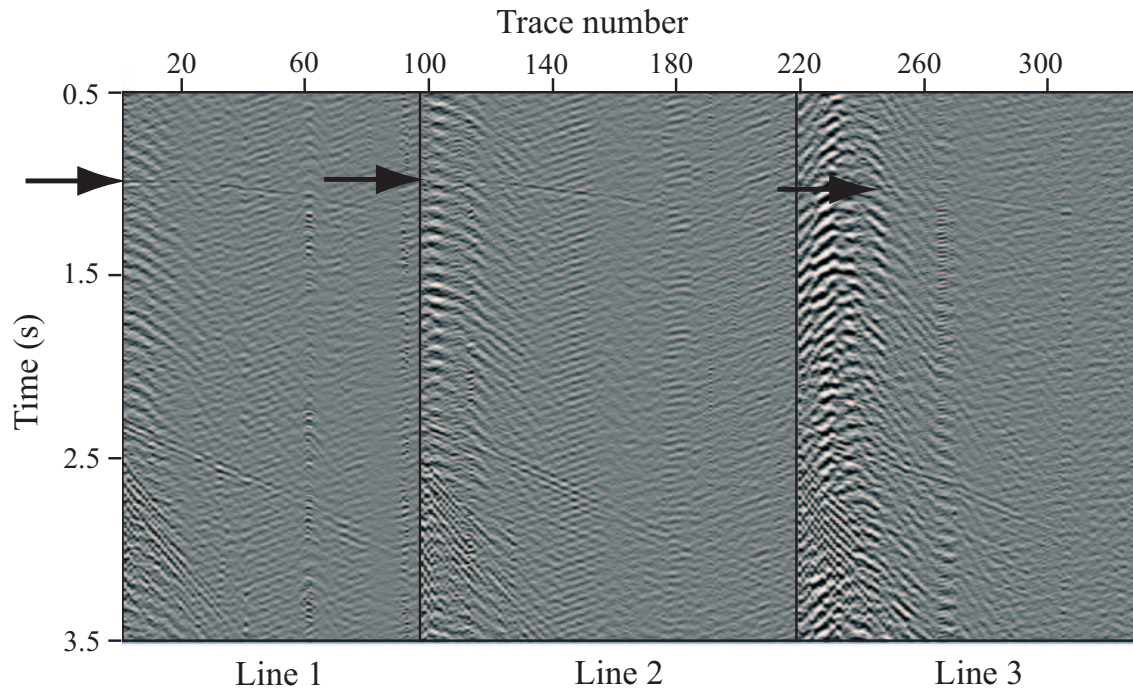


Figure 13: Seismic sections of lines 1-3 for shot 1. First arrivals are indicated by arrows.

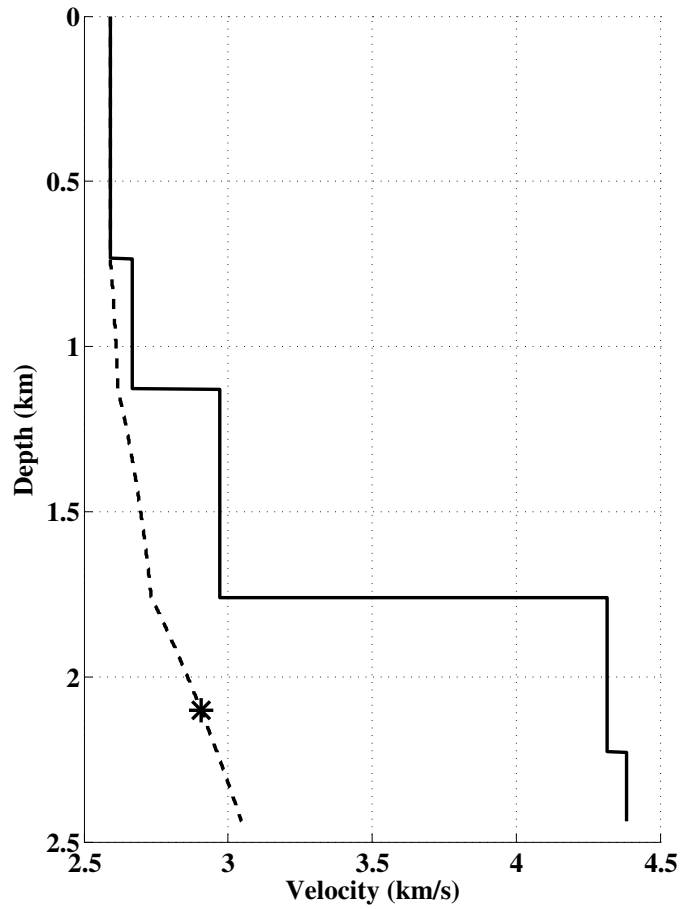


Figure 14: 1D vertical P-wave velocity profile of the study area. Interval velocity is given by the continuous line and the dashed line is the effective vertical velocity. Asterisk represents the effective velocity ( $V_{P0} = 2906$  m/s) with the source located at 2100 m, depth of perforation shots.

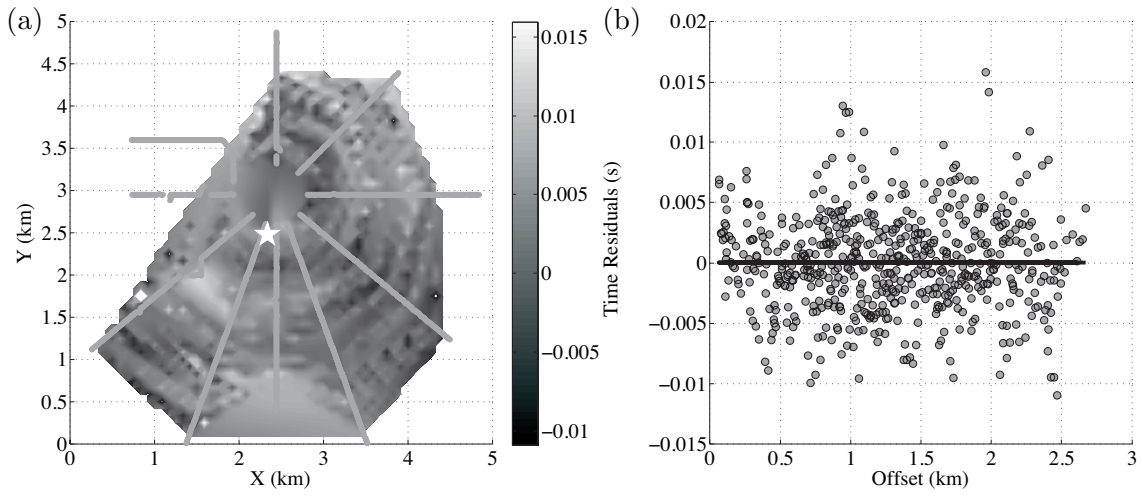


Figure 15: (a) Contour plot showing the time residuals from inversion of field data (shot 1); the straight gray lines represent the 10 arms of receivers of the Fracstar and the white star is the source location. (b) Time residuals of the perforation shot 1 of picked arrival times vs offset.

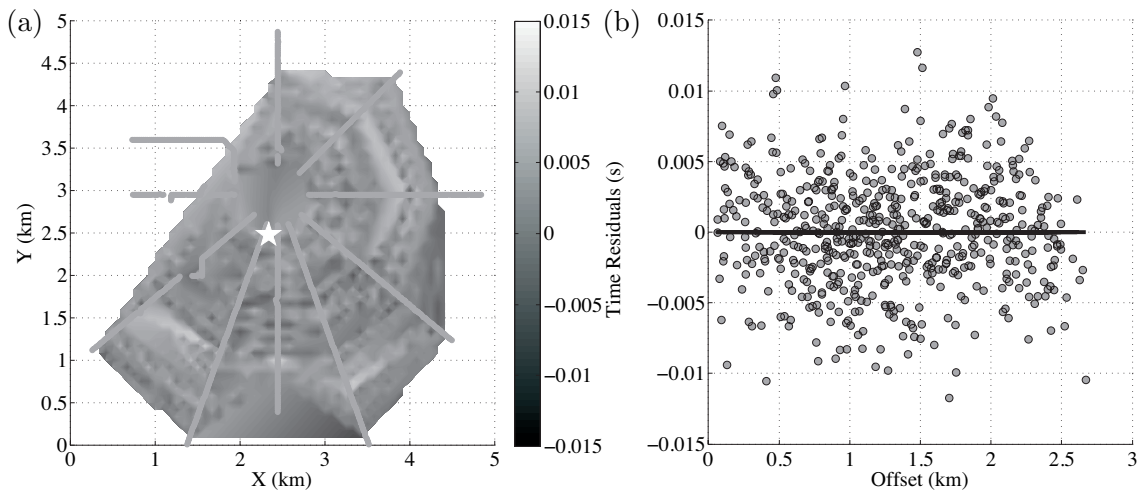


Figure 16: (a) Contour plot showing the time residuals from inversion of synthetic data; the straight gray lines represent the 10 arms of receivers of the Fracstar and the white star is the source location. (b) Time residuals of the perforation shot 1 of synthetic arrival times vs offset.